HAX1 impact on collective cell migration, cell adhesion, and cell shape is linked to the regulation of actomyosin contractility

Anna Balcerak[a,†], Alicja Trebinska-Stryjewska[a,b,†], Maciej Wakula[a], Mateusz Chmielarczyk[a], Urszula Smietanka[a], Tymon Rubel[c], Ryszard Konopinski[a], Ewelina Macech-Klicka[a], Renata Zub[a], and Ewa Anna Grzybowska[a,*]

[a]The Maria Sklodowska-Curie Institute—Oncology Center, 02-781 Warsaw, Poland; [b]Biomedical Engineering Centre, Institute of Optoelectronics, Military University of Technology, 00-908 Warsaw, Poland; [c]Institute of Radioelectronics and Multimedia Technology, Warsaw University of Technology, 00-665 Warsaw, Poland

ABSTRACT **HAX1 protein is involved in the regulation of apoptosis, cell motility and calcium homeostasis. Its overexpression was reported in several tumors, including breast cancer. This study demonstrates that HAX1 has an impact on collective, but not single-cell migration, thus indicating the importance of cell–cell contacts for the HAX1-mediated effect. Accordingly, it was shown that *HAX1* knockdown affects cell–cell junctions, substrate adhesion, and epithelial cell layer integrity. As demonstrated here, these effects can be attributed to the modulation of actomyosin contractility through changes in RhoA and septin signaling. Additionally, it was shown that HAX1 does not influence invasive potential in the breast cancer cell line, suggesting that its role in breast cancer progression may be linked instead to collective invasion of the epithelial cells but not single-cell dissemination.**

Monitoring Editor
Jonathan Chernoff
Fox Chase Cancer Center

Received: May 30, 2019
Revised: Oct 15, 2019
Accepted: Oct 18, 2019

INTRODUCTION

HAX1 is a multifunctional protein involved in regulating apoptosis, cell migration, and calcium homeostasis, but the molecular mechanisms underlying these effects are still unclear. HAX1 deficiency in humans leads to severe congenital neutropenia (Kostmann disease, SCN3) caused by maturation arrest of neutrophils (Klein *et al.*, 2007). Conversely, HAX1 overexpression has been observed in psoriasis (Mirmohammadsadegh *et al.*, 2003) and several human cancers (Ramsay *et al.*, 2007; Kwiecinska *et al.*, 2011; Li *et al.*, 2013, 2015; Wei *et al.*, 2014; Wang *et al.*, 2015), including breast cancer (Trebinska *et al.*, 2010). Sheng and Ni (2015) suggested that HAX1 is important for breast cancer progression.

Although HAX1's ability to attenuate apoptosis (Cilenti *et al.*, 2004; Han *et al.*, 2006; Chao *et al.*, 2008; Yan *et al.*, 2015) and promote cell migration should provide a relatively simple explanation for its overexpression in cancer, detailed analysis of its properties suggests that its function is not as straightforward as it may seem. Our recent results suggest that HAX1's role in regulating apoptosis is cell type and stimulus specific and, overall, not as prominent as expected, with the most pronounced effect observed on calcium-dependent apoptosis (Trebinska *et al.*, 2014). Reports on the effect of HAX1 on cell migration are not entirely consistent and somewhat contradictory; Radhika *et al.* (2004) suggested that Gα13-dependent cell motility is increased by HAX1, while Ramsay *et al.* (2007) described αvβ6-dependent migration which required HAX1 to regulate clathrin-mediated endocytosis of αvβ6 integrins. Cavnar *et al.* (2011) and Liu *et al.* (2015) have shown that HAX1 depletion in neutrophils and skin epidermal cells, respectively, impairs cell migration and stabilizes adhesion, but Pedersen *et al.* (2014) did not observe the effect of *HAX1* knockdown (KD) on cell migration in

This article was published online ahead of print in MBoC in Press (http://www.molbiolcell.org/cgi/doi/10.1091/mbc.E19-05-0304) on October 23, 2019.

†These authors contributed equally to the work.

The authors declare no conflicts of interest.

Authors' contributions: A.B., A.T.S., M.W., M.C., U.S., E.M.K., R.K., and R.Z. performed experiments; A.T.S., E.G., and M.W. performed statistical analysis; T.R. performed mass spectrometry data analysis; A.T.S. and E.G. designed the research and edited the manuscript for intellectual content.

*Address correspondence to: Ewa Anna Grzybowska (ewag@coi.waw.pl).

Abbreviations used: CSI, cell shape index; CTC, circulating tumor cells; ECM, extracellular matrix; EMT, epithelial-mesenchymal transition; FBS, fetal bovine serum; FCF, forchlorfenuron; IP, immunoprecipitation; KD, knockdown; PCC, Pearson's correlation coefficient; STRING, Search Tool for the Retrieval of Interacting Genes/Proteins; TCE, 2,2,2-trichloroethanol.

breast cancer cell lines. Gomathinayagam *et al.* (2014) and Li *et al.* (2015) also confirmed the effect of *HAX1* KD on cell migration in ovarian carcinoma cells and cutaneous squamous carcinoma cells, respectively.

To date, the proposed molecular mechanisms behind these effects included two main pathways: integrin endocytosis (Ramsay *et al.*, 2007) and the regulation of small GTPases from the Rho family, which governs cell migration (Radhika *et al.*, 2004; Cavnar *et al.*, 2011; Gomathinayagam *et al.*, 2014). There are also several reports describing HAX1 associations with the cytoskeleton; it was shown to interact with cortactin (Gallagher *et al.*, 2000; Gomathinayagam *et al.*, 2014), regulate actin nucleation through Arp2/3 (Zhang *et al.*, 2016), influence vimentin (Al-Maghrebi *et al.*, 2002; Zayat *et al.*, 2015), and interact with microtubule end-binding protein (Liu *et al.*, 2015). HAX1 was also suggested to regulate cell invasion (Ramsay *et al.*, 2007; Mekkawy *et al.*, 2011; Sun *et al.*, 2012; Li *et al.*, 2015). Overall, although the accumulated evidence points to HAX1 involvement in regulating cell migration, invasion, and, ultimately, metastasis, the exact mechanisms by which this effect is executed are not quite clear at the moment.

The results presented in this study demonstrate that HAX1 has an impact on collective migration of the epithelial cell layer in breast cancer cell lines, which is linked to changes in cell–cell and cell–substrate adhesion, monolayer integrity, and altered actomyosin contractility. Additionally, this study demonstrates that HAX1 deficiency has no effect on invasion in the breast cancer cell line. These results suggest that the HAX1 role in breast cancer progression should not be attributed to the epithelial-mesenchymal transition (EMT)-driven single-cell dissemination in a classic metastatic cascade, but rather to the collective cell invasion or circulating tumor cells' (CTC) cluster formation.

RESULTS

HAX1 deficiency affects collective migration of the epithelial cell layer

To assess HAX1 impact on cell migration, two stable *HAX1* KDs and the two appropriate controls were generated for each of the breast cancer cell lines with different characteristics: MCF7 and MDA-MB-231 (Supplemental Figure S1A; Thompson *et al.*, 1992). The MCF7 represents a typical epithelial cell line, corresponding to luminal A breast cancer, with the strong cell–cell junctions, low migratory potential, and no invasive potential. HAX1 expression is elevated in the MCF7 cell line compared to nontumorigenic MCF10A cells (Supplemental Figure S1B; Yang *et al.*, 2017). MDA-MB-231 represents breast cancer cells after EMT and corresponds to triple-negative breast cancer. As a post-EMT cell line, it has a very high migratory and invasive potential. Cell lines were subjected to three different assays: two assays able to measure collective cell migration of the monolayer (the classical wound healing assay and radius cell migration assay) and the transwell migration assay. Although these assays do not differentiate by design between collective and single-cell migration, wound healing and radius assays are able to measure collective migration of the confluent, integrated monolayer (Li *et al.*, 2016), while in the transwell assay, this specific type of migration is precluded by the pore diameter of 8 μm, only allowing for single-cell passage. The results, presented in Figure 1, indicate that, for MCF7 epithelial cells, *HAX1* KD significantly affects cell migration measured by collective migration assays (Figure 1, A–F; Supplemental Figure S2, A and B), while in the transwell cell assay, despite using the same cell lines, there is no significant difference (Figure 1J). To confirm these findings, similar experiments (wound healing assay and radius migration assay) were performed in the T47D epithelial breast cancer cell line, and the same effect was observed (Supplemental Figure S2, D and E). Moreover, to demonstrate that the HAX1 effect is not dependent on the method of silencing, a stable MCF7-based cell line with *HAX1* KD was established using short hairpin RNA (shRNA) and its migration was compared with the appropriate control to the same effect (Supplemental Figure S2C). Quantification of these results indicated that in MCF7 cell lines with *HAX1* KD migration is reduced by 50%. To eliminate the effect of proliferation, the migration of MCF7 cell line with proliferation inhibitor cytarabine was compared with the migration of untreated cells, and no difference was observed (Supplemental Figure S2F). MDA-MB-231 cells, although primarily epithelial, have a mesenchymal-like phenotype, which allows collective migration due to sparse and transient cell–cell contacts, but not as a fully integrated cell layer as in the case of epithelial cells (Clark and Vignjevic, 2015; Campbell and Casanova, 2016). *HAX1* KD had no effect on cell migration in MDA-MB-231-based cell lines in all three assays (wound healing, radius, and transwell assay; Figure 1, G–J), indicating that HAX1 regulates only integrated, collective migration of the monolayer, weakened in MDA-MB-231 cells by the lower number of cell–cell contacts. Interestingly, wound-healing assay for *HAX1* overexpressing the MDA-MB-231 cell line demonstrated ~1.5× increase in migration compared to the control cell line (Supplemental Figure S2, G and H), suggesting that it may enhance collective migration in these cells. Overall, HAX1 depletion was found to be important for cell migration only in the assays able to measure collective migration of the whole monolayer, pointing to the role of cell–cell contacts in HAX1-mediated regulation.

HAX1 does not promote cell invasion in breast cancer cells

Cell migration is often linked to enhanced invasive properties, and the impact on invasion was suggested for HAX1 by some reports (Ramsay *et al.*, 2007; Sun *et al.*, 2012; Hu *et al.*, 2018). Accordingly, invasive properties of HAX1-deficient cells were tested by invasion assays (Figure 1K) and collagen zymography (Figure 1L). These assays were performed only for MDA-MB-231-derived cell lines, since epithelial MCF7 cells do not have invasive properties. These experiments demonstrated that HAX1 KD does not affect invasive properties assessed by these assays.

HAX1 KD affects cell–cell junctions

Differential response of HAX1-deficient cells in migration assays suggested that strong cell–cell contacts required for collective migration of the monolayer may play a role in HAX1-mediated regulation. The integrity of the two major types of cell–cell contacts (adherens junctions and desmosomes) was tested in MCF7-based cell lines by calcium switching experiments. All cell–cell contacts are calcium-dependent. To test whether HAX1 has an effect on both types of junctions, confluent, mature cell layers were treated with EGTA (ethylene glycol-bis(2-aminoethylether)-*N*,*N*,*N*′,*N*′-tetraacetic acid, calcium chelator) and the effect of calcium depletion was compared in *HAX1* KDs versus controls by E-cadherin (adherens junctions) and junction plakoglobin (desmosomes) staining. The difference could be observed even in untreated culture, with HAX1-deficient cells exhibiting delocalized junction proteins in the cytoplasm (Figure 2A), while the amount of both proteins quantified by Western blot was slightly decreased for E-cadherin in *HAX1* KDs and the same for plakoglobin (Supplemental Figure S3). Calcium depletion experiments demonstrated that cell–cell junctions in control cells display more resistance to calcium removal than in *HAX1* KDs. Control cells still formed a monolayer, with occasional delocalization of junction proteins, while *HAX1* KDs exhibited cell layer disruption and cell rounding (Figure 2A; Supplemental Figure S4).

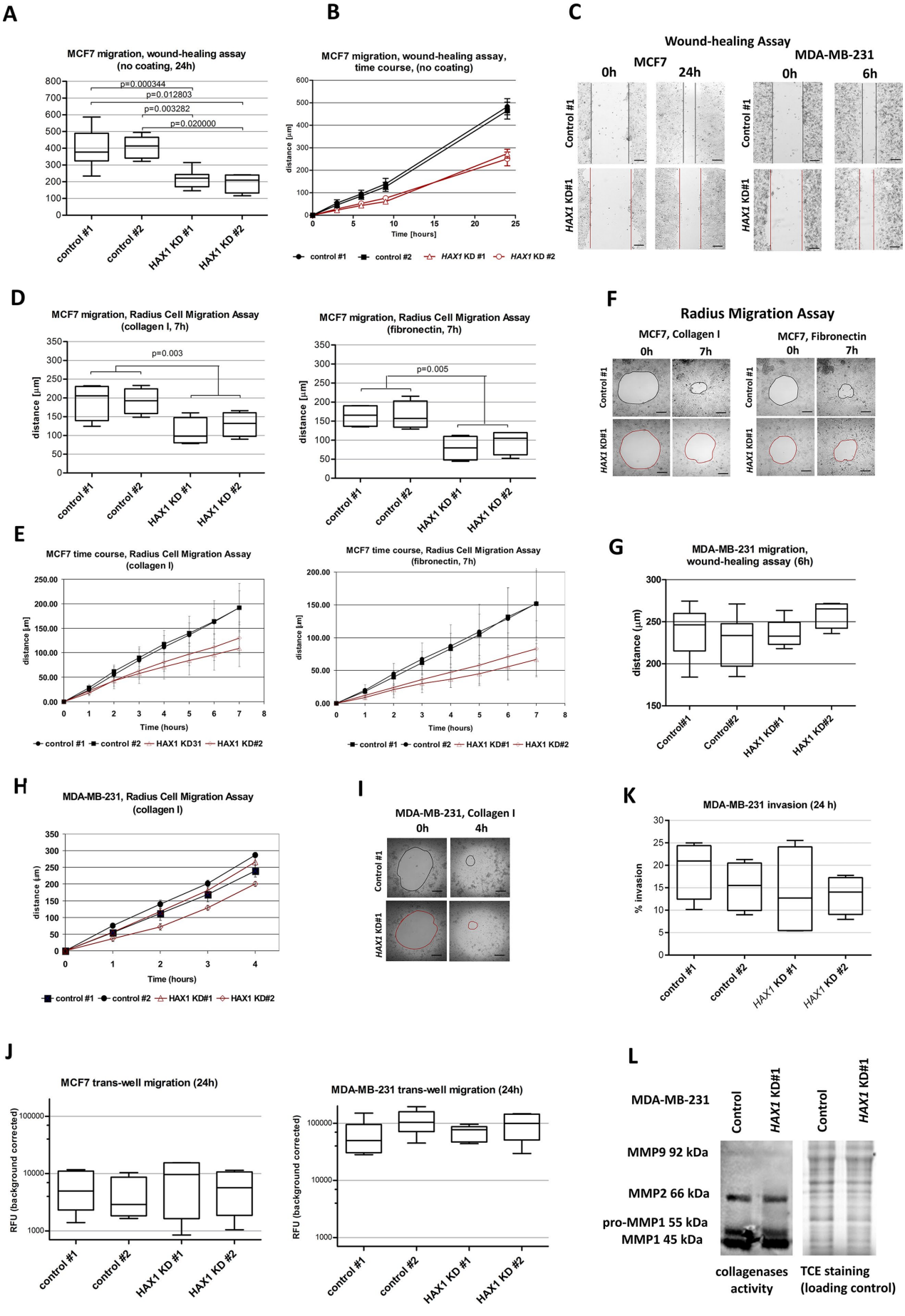
A
MCF7 migration, wound-healing assay (no coating, 24h)
p=0.000344
p=0.012803
p=0.003282
p=0.020000
control #1
control #2
HAX1 KD #1
HAX1 KD #2
B
MCF7 migration, wound-healing assay, time course, (no coating)
distance [µm]
Time [hours]
control #1
control #2
HAX1 KD #1
HAX1 KD #2
C
Wound-healing Assay
MCF7
MDA-MB-231
0h
24h
0h
6h
Control #1
HAX1 KD#1
D
MCF7 migration, Radius Cell Migration Assay (collagen I, 7h)
p=0.003
distance [µm]
MCF7 migration, Radius Cell Migration Assay (fibronectin, 7h)
p=0.005
F
Radius Migration Assay
MCF7, Collagen I
MCF7, Fibronectin
0h
7h
E
MCF7 time course, Radius Cell Migration Assay (collagen I)
distance [µm]
Time (hours)
control #1
control #2
HAX1 KD31
HAX1 KD#2
MCF7 time course, Radius Cell Migration Assay (fibronectin, 7h)
G
MDA-MB-231 migration, wound-healing assay (6h)
distance (µm)
Control#1
Control#2
HAX1 KD#1
HAX1 KD#2
H
MDA-MB-231, Radius Cell Migration Assay (collagen I)
distance (µm)
Time (hours)
control #1
control #2
HAX1 KD#1
HAX1 KD#2
I
MDA-MB-231, Collagen I
0h
4h
Control #1
HAX1 KD#1
K
MDA-MB-231 invasion (24 h)
% invasion
control #1
control #2
HAX1 KD #1
HAX1 KD #2
J
MCF7 trans-well migration (24h)
RFU (background corrected)
MDA-MB-231 trans-well migration (24h)
control #1
control #2
HAX1 KD #1
HAX1 KD #2
L
MDA-MB-231
Control
HAX1 KD#1
Control
HAX1 KD#1
MMP9 92 kDa
MMP2 66 kDa
pro-MMP1 55 kDa
MMP1 45 kDa
collagenases activity
TCE staining (loading control)

To further explore differences in the strength of cell–cell contacts between *HAX1* KDs and controls in MCF7 cells, cell fragmentation assay with dispase II was performed. Fully confluent, mature cell layers were detached from the substrate by dispase II treatment and subjected to mechanical stress. The fragments were counted at designated time points. The results demonstrated that control monolayers largely resisted fragmentation, while *HAX1* KDs did not exhibit the same resistance to mechanical stress (Figure 2B).

HAX1 KD promotes cell–substrate adhesion and actin stress fibers formation but affects cortical actin organization

Both, cell–cell and cell–substrate adhesions have a role in the regulation of cell migration and have to be properly balanced, especially during coordinated movement of the epithelial cell layer (Collins and Nelson, 2015).

The size and quantity of focal adhesions were assessed in MCF7 *HAX1* KDs versus controls. Focal adhesions were stained with paxillin, and their number and area were quantified using ImageJ. The results revealed that *HAX1* KDs focal adhesions tend to be slightly more numerous and significantly larger in size (Figure 3, A and B), suggesting differences in cell–substrate adhesion between these cell lines. Increased size of focal adhesions in *HAX1* KDs is in line with the increase in actin fiber formation, anchored in focal adhesions. F-actin organization was compared at the basal plane in control and *HAX1* KD cell lines, revealing more distinctive actin fibers in *HAX1* KD (Figure 3C).

Actin staining was also compared in apical plane of control and HAX1-deficent cells, revealing disrupted organization and irregular distribution of cortical actin (Figure 3D). These changes corresponded to changes in monolayer organization, observed for junction proteins (Figure 3D; also visible in Figure 4A).

HAX1 KD affects cell shape via myosin II

The organization of the monolayer of *HAX1* KD versus control (MCF7) displayed striking differences not only in the distribution of junction proteins and actin but also in the general layout of the monolayer, including changes in cell shape. Cell shape was assessed using the circularity index (also called cell shape index; CSI). CSI measurements, performed for 150–400 cells, indicated that control cell layers were more regular, with a CSI of ~0.7–0.9 (skewness: –0.701; kurtosis: 0.209), while in *HAX1* KDs, cell shape was more varied (CSI spectrum: 0.1–1, more uniform distribution, skewness: –0.055;, kurtosis: –0.850; Figure 4, A and B; also visible in Figure 3D). Blebbistatin (myosin II inhibitor) and Y27632 (ROCK inhibitor) treatments of *HAX1* KD cells partially restored regular monolayer, as evidenced by the comparison of cumulative distribution frequency plots, which are much more similar after either treatment (Figure 4B), suggesting that HAX1 may be involved in the regulation of myosin II. Accordingly, treatment with blebbistatin significantly reversed the effect of *HAX1* KD on migration, resulting in the lack of statistical difference between *HAX1* KD and control after treatment (Figure 4C, top panel). The same effect was observed for Y27632 (Figure 4C bottom panel). Both inhibitors enhance the speed of collective migration in wound healing assay.

RhoA-ROCK pathway and septins are involved in HAX1-mediated regulation of actomyosin contractility

To further dissect the impact of HAX1 deficiency on myosin II activity, myosin light chain phosphorylation was tested in control and HAX1 KD, showing, in line with blebbistatin and Y27632 effects, increased phosphorylation in HAX1-deficent cells (Figure 5A). To explore possible molecular mechanisms behind this and the other observed effects, RhoA-ROCK signaling was investigated in HAX1-deficient cells as the main pathway controlling cell shape, actomyosin contractility, and stress fiber formation. It has been established that the increase in RhoA activity in the *HAX1* KD cell line was not prominent (Figure 5B), suggesting that it cannot be the only factor responsible for the observed effect. In a search for the other factors potentially involved in the regulation of myosin II, targeted immunoprecipitation (IP) and subsequent mass spectrometry of proteins coprecipitating with HAX1 were performed in the MCF7 cell line. The results revealed a large subset of cytoskeletal and regulatory proteins involved in actin bundling, actomyosin ring formation and actomyosin contractility, microtubule assembly, cytokinesis, and cell movement (Table 1). The most prominent group among these proteins were septins, filament-forming GTPases related to the Ras superfamily, which clustered together in a STRING (Search Tool for the Retrieval of Interacting Genes/Proteins; string-db.org) protein interaction network analysis (Supplemental Figure S5). To assess the possibility of the interplay between septins and HAX1, septin inhibitor forchlorfenuron (FCF) was used in control and HAX1-deficient cells. Partial but significant colocalization of septin 7 and HAX1 was

FIGURE 1: HAX1 impact on cell migration in breast cancer cell lines. The effect of *HAX1* KD on cell migration in comparison to the appropriate controls in epithelial MCF7 and mesenchymal-like MDA-MB-231 breast cancer cell lines. For every cell line, two independent KDs and two controls were tested; n = the number of biological replicates. (A) Wound-healing assay on uncoated surface for MCF7-based cell lines (n = 4–18); each biological replicate represents an average of seven different measurement points. Statistical significance was assessed by Kruskal–Wallis test by ranks for multiple comparisons and post-hoc Dunn test. (B) Time series of wound healing assay are for MCF7-based cell lines, and time points are as indicated, error bars: SD, n = 4. (C) Representative images of the wound healing assay in MCF7-based cell lines (left) and MDA-MB-231-based cell lines (right) in designated time points. (D) Radius cell migration assay for MCF7 control and *HAX1* KD cell lines seeded on collagen I (n = 4) and fibronectin (n = 4). Statistical significance was assessed by one-way ANOVA and planned comparisons for groups (planned contrast). (E) Time series of radius cell migration assay for MCF7-based cell lines, time points, and coating as indicated, error bars: SD, n = 4. (F) Representative images of the radius cell migration assay in MCF7-based cell lines on collagen I and fibronectin (7 h) (G) Wound-healing assay on uncoated surface for MDA-MB231-based cell lines (n = 4) shows no statistically significant difference (Kruskal–Wallis). (H) Time series of radius cell migration assay for MDA-MB-231-based cell lines, collagen I (n = 4). (I) Representative images of the radius cell migration assay in MDA-MB-231 on collagen I. (J) Trans-well cell migration assay in FBS gradient (0.5%–10% FBS) for MCF7-based cell lines (n = 5) and MDA-MB-231-based cell lines (n = 5). RFU-relative fluorescence units, log scale, and background corrected for medium. Statistical significance assessed by Kruskal–Wallis. (K) Matrigel invasion assay (n = 4) in MDA-MB-231 cell lines presented as the percentage of invasion (100 × mean RFU of invaded cells through Matrigel-coated membrane/mean RFU of migrated cells through uncoated membrane). Statistical significance assessed by Kruskal–Wallis. (L) Collagen zymography showing no effect of *HAX1* KD for the activity of collagenases.

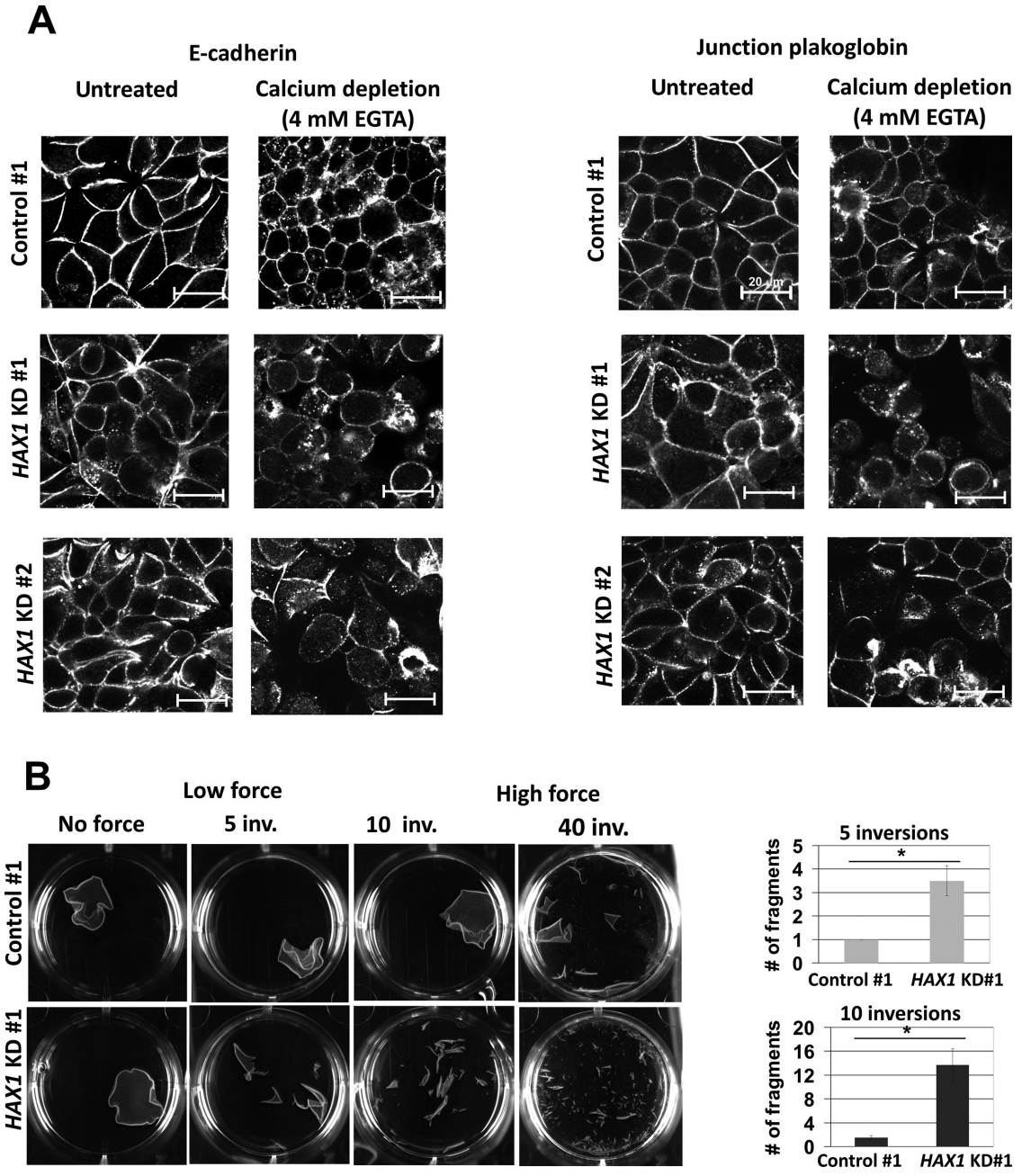

FIGURE 2: Cell–cell contacts are compromised in HAX1-deficient monolayers of MCF7 cells. (A) Mature, confluent cell layers of control and *HAX1* KD cell lines before and after calcium depletion. Staining: E-cadherin and junction plakoglobin; panels left to right: untreated and treated with 4 mM EGTA for 30 min. Bar: 20 μm. (B) Fragmentation assay: confluent cell layers were treated by dispase II (2.4 U/ml, 50 min) and subjected to mechanical force: low (5–10 inversions of the plates) and high (40 inversions). Right panel: fragment count after low force stress; error bars represent SEM. The experiment was done in triplicate. Statistical significance was assessed by two-tailed Student's *t* test, * marks $p < 0.05$.

detected in both untreated and FCF-treated cells, with Pearson's correlation coefficient (PCC) and the two Mander's overlap coefficients (M1, M2) not significantly different before and after FCF treatment (Figure 5C). HAX1-deficient cells did not show any significant changes in actin cytoskeleton after FCF treatment, but in control cells actin stress fibers were more pronounced (Figure 5D). Moreover, after FCF treatment, there was no statistical difference in migration of control and HAX1-deficient cells—as with blebbistatin and Y27632—although these inhibitors act oppositely on migration (Figures 4C and 5E). These results indicate again that control cells are more affected by FCF, with the phenotype after the treatment resembling HAX1-deficient cells (Figure 5, D and E). To test the effect of *HAX1* KD on septin morphology, staining of SEPT2 and SEPT7 (the highest scoring hits in mass spectrometry) was compared in control and HAX1-deficient cells, revealing differences in both cases. For SEPT2, in control cells, the staining resembles cortical actin, while in *HAX1* KD, the pattern is not as regular. SEPT7 fibrils are not very pronounced in control cells, while in *HAX1* KD thick SEPT7 fibrils can be occasionally observed (Figure 5F). Overall, the results presented here suggest a model of HAX1-mediated

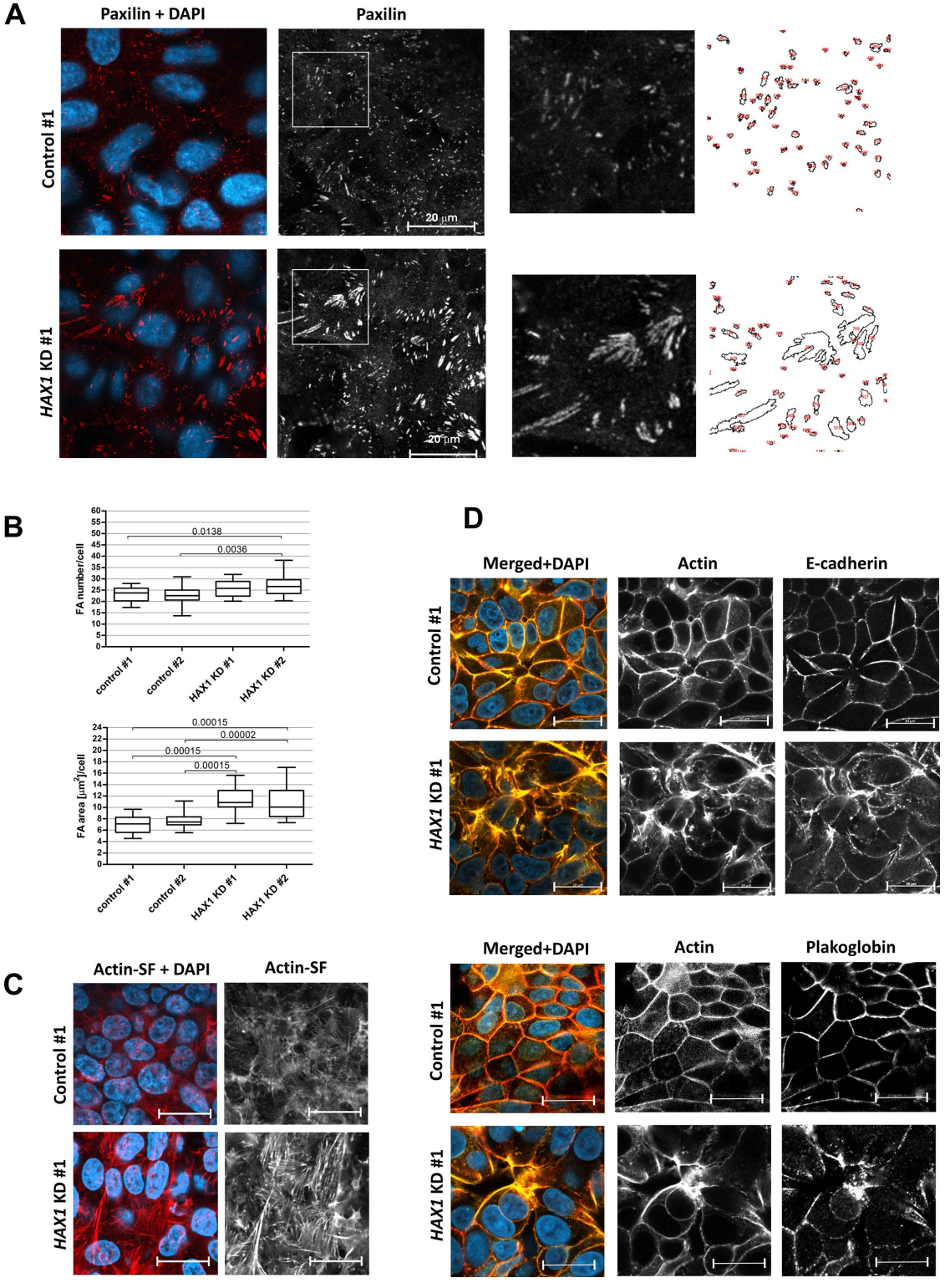

FIGURE 3: *HAX1* KD affects cell–substrate adhesion and actin cytoskeleton organization in MCF7 cells. Comparison of control cells and *HAX1* KD. (A) Paxillin staining. Insets show zoomed versions of boxed areas, along with examples of ImageJ-generated FAs count. (B) Differences in FAs number and area per cell in the studied cell lines. The measurements were performed for ~2500 cells per cell line (20 independent fields of vision, 63× objective, bar: 20 μm). Statistical significance was assessed by one-way ANOVA and Tukey. (C) Comparison of actin stress fibers at the basal region of the cell. Bar: 20 μm. The *z*-axis for stress fiber detection adjusted to match *z*-axis with visible paxillin. (D) Comparison of cortical actin distribution and organization in apical plane of *HAX1* KD and control cells. The *z* axis adjusted to match junction proteins; E-cadherin (left panel) and junction plakoglobin (right panel). Bar: 20 μm.

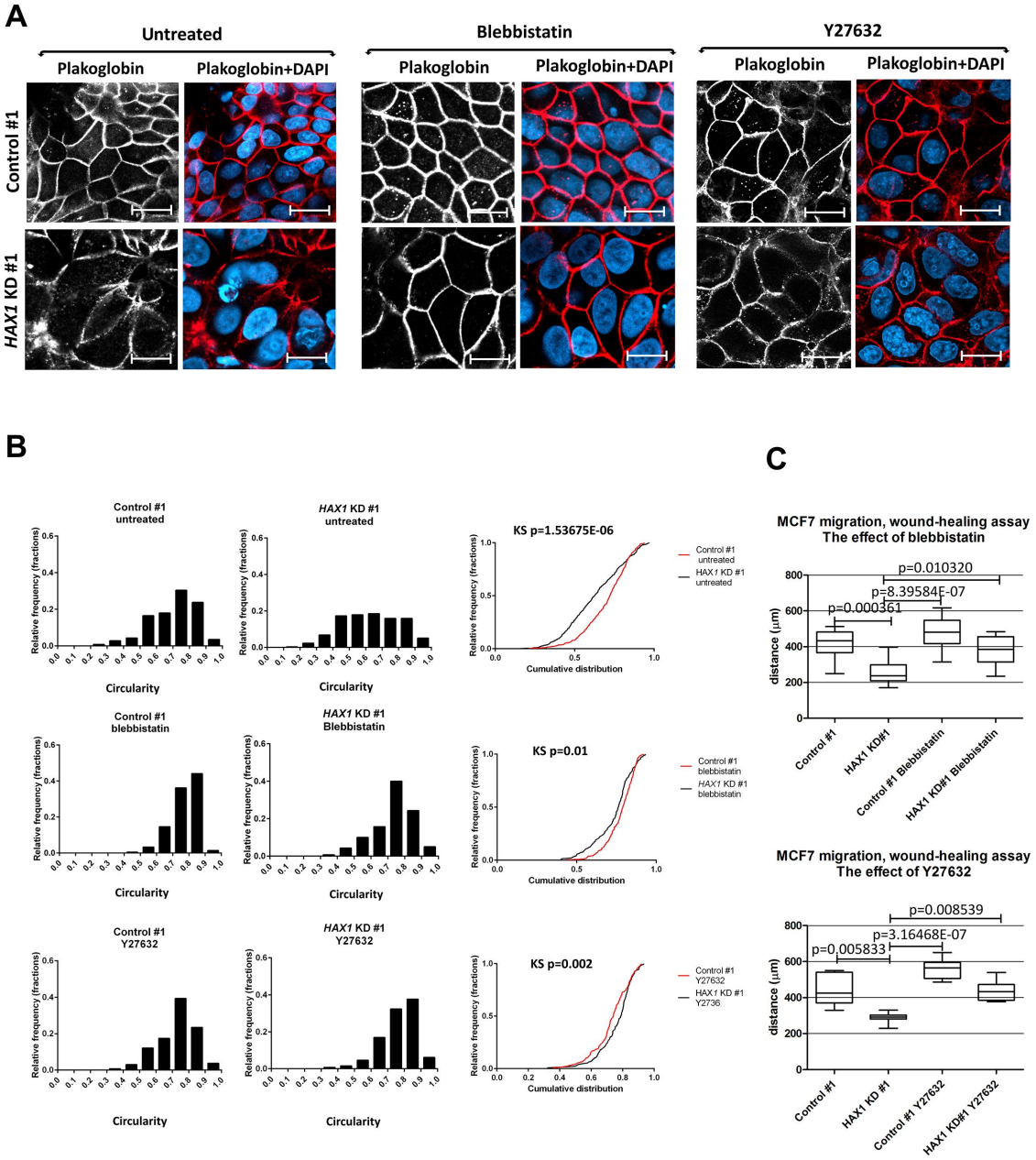

FIGURE 4: *HAX1* KD affects cell shape through myosin II. (A) The effect of HAX1 KD on cell shape in the epithelial cell layer in untreated cells (left panel) and cells treated with blebbistatin (50 µM, 12 h, middle panel) and Y27632 (10 µM, 1 h, right panel); staining: junction plakoglobin (red), nuclei (DAPI, blue). (B) Cell shape distribution presented as a histogram of circularity (CSI); bin width: 0.1, calculated for 150–400 cells (three to five independent fields of vision, 63× objective, bar: 20 µm) for each indicated cell line. Cumulative frequency distribution plots compared for the control and *HAX1* KD#1 for the untreated and blebbistatin and Y27632-treated cells. Differences in the distribution were assessed by Kolmogorow–Smirnov two-sample test. (C) The effects of blebbistatin (50 µM, 12 h, top panel) and Y27632 (10 µM, 1 h, bottom panel) on cell migration of HAX1-deficient vs. control cells in wound-healing assay ($n = 14$ and $n = 10$, respectively). Both inhibitors reduce the difference in migration of control vs. HAX1-deficient cells, which becomes insignificant after the treatment. The results shown as box plots with median values, interquartile range, maximum and minimum. Statistical significance was assessed by Kruskal–Wallis and Dunn.

regulation in which both Rho-ROCK pathway and septins are involved in the regulation of myosin II (Figure 5G).

DISCUSSION

Although HAX1 protein has been implicated in many cellular processes, its molecular mechanisms of action remain elusive. The HAX1 role in cancer progression is proposed to be mediated by regulating apoptosis and/or cell migration and invasion. In this study, we investigated the HAX1 impact on cell adhesion, migration, and invasion in breast cancer cell lines. Using our model cell lines with *HAX1* KD, we demonstrated that HAX1 affects only collective cell migration of the monolayer. Since cell–cell contacts are crucial for the efficient collective migration of the monolayer, but have no role in the mesenchymal-type individual cell migration, we

concluded that HAX1 promotes strong cell–cell contacts. Accordingly, we demonstrated that cell–cell contacts in HAX1-deficient cells are compromised, with delocalization of junction proteins and enhanced sensitivity to calcium depletion and mechanical stress. Thus, by promoting strong cell–cell contacts, HAX1 may contribute to the full integration of migrating monolayer.

To address HAX1 impact on invasion, suggested by some reports (Ramsay *et al.*, 2007; Sun *et al.*, 2012; Hu *et al.*, 2018), we performed invasion and matrix metalloproteinase activity assays, demonstrating that there were no differences between control and HAX1-deficient cell lines. We also did not observe any effect of HAX1 deficiency on EMT markers' expression (data not shown). Overall, presented results point to HAX1 role in enhancing cell–cell junctions (the hallmark of epithelial cells) and indicate no role in invasion. Accordingly, it does not seem probable for HAX1 to be responsible for the EMT-driven metastatic spread of single, mesenchymal-like cells. However, enhanced collective migration of HAX1-overexpressing breast cancer cells may promote invasion of the surrounding tissues. More importantly, recent reports demonstrate that in breast cancer the dissemination is caused mostly by highly invasive clusters of CTCs, which partially retain epithelial phenotype, including plakoglobin-based cell–cell junctions (Aceto *et al.*, 2014; Cheung *et al.*, 2016) and HAX1 is on the list of up-regulated transcripts in CTC clusters versus single CTCs (Aceto *et al.*, 2014). Thus, the HAX1 impact on breast cancer progression may include enhanced collective invasion, CTC clusters formation/maintenance, or some other EMT-independent factor.

As reported here, HAX1 influences not only cell–cell but also cell–substrate adhesion. In HAX1-deficient cells, focal adhesions are slightly more numerous and significantly larger, while actin stress fibers originating in these focal adhesions are more pronounced. These observations are consistent with the results of Radhika *et al.* (2004) and Zhang *et al.* (2016). However, on an apical plane, the cortical actin network in HAX1-deficient cells is severely disturbed. Since the two types of adhesion are interrelated and coordinated by the actin cytoskeleton (Collins and Nelson, 2015; Bachir *et al.*, 2017), HAX1 may be implicated in the integration of cell–cell and cell–substrate adhesion sites with actin network.

Moreover, changes in cell shape and aberrations in the organization of the monolayer observed in HAX1-deficient cells indicate alterations in actomyosin contractility, since it is the main cell-shaping force. Restoration of a relatively regular monolayer and the speed of collective migration in *HAX1* KD after blebbistatin and Y27632 treatments imply that actomyosin contractility is increased in these cells and contributes to the disruption of monolayer integrity. These results are in line with an observation that excessive actomyosin activity is detrimental to collective cell migration (Hidalgo-Carcedo *et al.*, 2011). The myosin light chain phosphorylation assay confirmed that myosin II activity is enhanced in HAX1-deficient cells. To further explain the molecular mechanisms of HAX1-mediated regulation, we analyzed the involvement of the RhoA-ROCK pathway, which controls both actomyosin contractility and stress fiber formation. HAX1 was previously reported to influence RhoA activity in neutrophils (Cavnar *et al.*, 2011). We have found that in MCF7 cells, HAX1 affects RhoA activity, but the effect is moderate, suggesting that this pathway is involved in HAX1-mediated regulation, but it cannot represent the only mechanism. In a search of the other potential myosin-affecting factors, we have characterized a set of the new HAX1 protein partners in MCF7 cells and focused on septins, filamentous GTPases related to the Ras superfamily, with a role in regulating focal adhesions, stress fibers, and mechanical tension (Spiliotis and Gladfelter, 2012; Burridge and Guilluy, 2016). Septins are known to bind and regulate actin and myosin II and, as a consequence, to modulate actomyosin contractility. Septins 7 and 9 were shown to inhibit myosin II (Smith *et al.*, 2015; Wasik *et al.*, 2017). The only known septin inhibitor/modulator, FCF, was used in this study and shown to reduce the difference in migration of HAX1-deficient and control monolayers. Interestingly, FCF-treated control cells resemble HAX1-deficient cells. Thus, as proposed in Figure 5G, if FCF releases septin inhibition of myosin II, leading to an excessive contractility, to fit the data, HAX1 should act in an opposite manner, leading to the suppression of actomyosin and less pronounced actin fibers. Paradoxically, these effects, combined with more robust cell–cell junctions (increased tensile forces) and more regular cell shape, may potentiate collective migration by promoting monolayer integrity and reducing traction force. Further research should determine whether HAX1 impact on septins relies on the modulation of their GTPase activity, which seems probable, since this protein is known to regulate the other GTPases from the Rho family (Radhika *et al.*, 2004; Cavnar *et al.*, 2011), closely related to septin GTPases.

Presented results indicate that HAX1-deficient cells display reduced cell–cell contacts, enhanced focal adhesions and stress fibers, and increased actomyosin contractility, which translates into slower collective migration. Further studies are needed to establish the exact molecular mechanisms behind this phenotype, but our preliminary results point to the role of septins. Medical implications of these results include clarification of the role of HAX1 in breast cancer metastasis, favoring its involvement in collective invasion or CTC clusters formation.

MATERIALS AND METHODS

Cell lines

MCF7 (American Type Culture Collection [ATCC]), MDA-MB-231 (ATCC), and T47D (DSMZ) human cell lines were used in the experiments. Cell lines were authenticated by Eurofins Genomics (Germany). Cells were grown in DMEM supplemented with 10% fetal bovine serum (FBS; Thermo Fisher Scientific). When indicated, cells were treated with 50 µM blebbistatin for 12 h, 10 µM Y27632 (ROCK inhibitor) for 1 h, or 5 or 15 µM FCF for 18 h.

Plasmids and constructs

SEPT7 cDNA was amplified using primers forward 5′-tcggatccATGTCGGTCAGTGCGAGATCCGCTG-3′ and reverse 5′-ctctagatTTAAAAGATCTTCCCTTTCTTC-3′ and cloned into pCR3-FLAG commercial vector using *Bam*HI and *Xba*I restriction sites. HAX1-GFP construct was described in Grzybowska *et al.* (2013).

HAX1 KD

Cell lines with *HAX1* KD were generated as described for HeLa cells by Grzybowska *et al.* (2013) using the BLOCK-iT Pol II miR RNAi Expression Vector system (Invitrogen). MCF7, T47D, and MDA-MB-231 cells were transfected with the silencing plasmid (pcDNA6.2-GW/EmGFP-miR-HAX1) using Lipofectamine 2000 (Invitrogen). The pcDNA6.2-GW/EmGFP-miR-neg plasmid (Invitrogen) was used to generate control cell lines. Single clones were isolated in 7.5 µg/ml blasticidin-supplemented medium. Levels of HAX1 protein were assessed by Western blotting. Two independent stable KDs and two controls were generated for each cell line. *HAX1* shRNA KD was generated using Sigma Mision pLKO.1 shRNA plasmid TRCN0000061777 and Mission pLKO.1-puro nontarget shRNA control, according to the manufacturer's instructions.

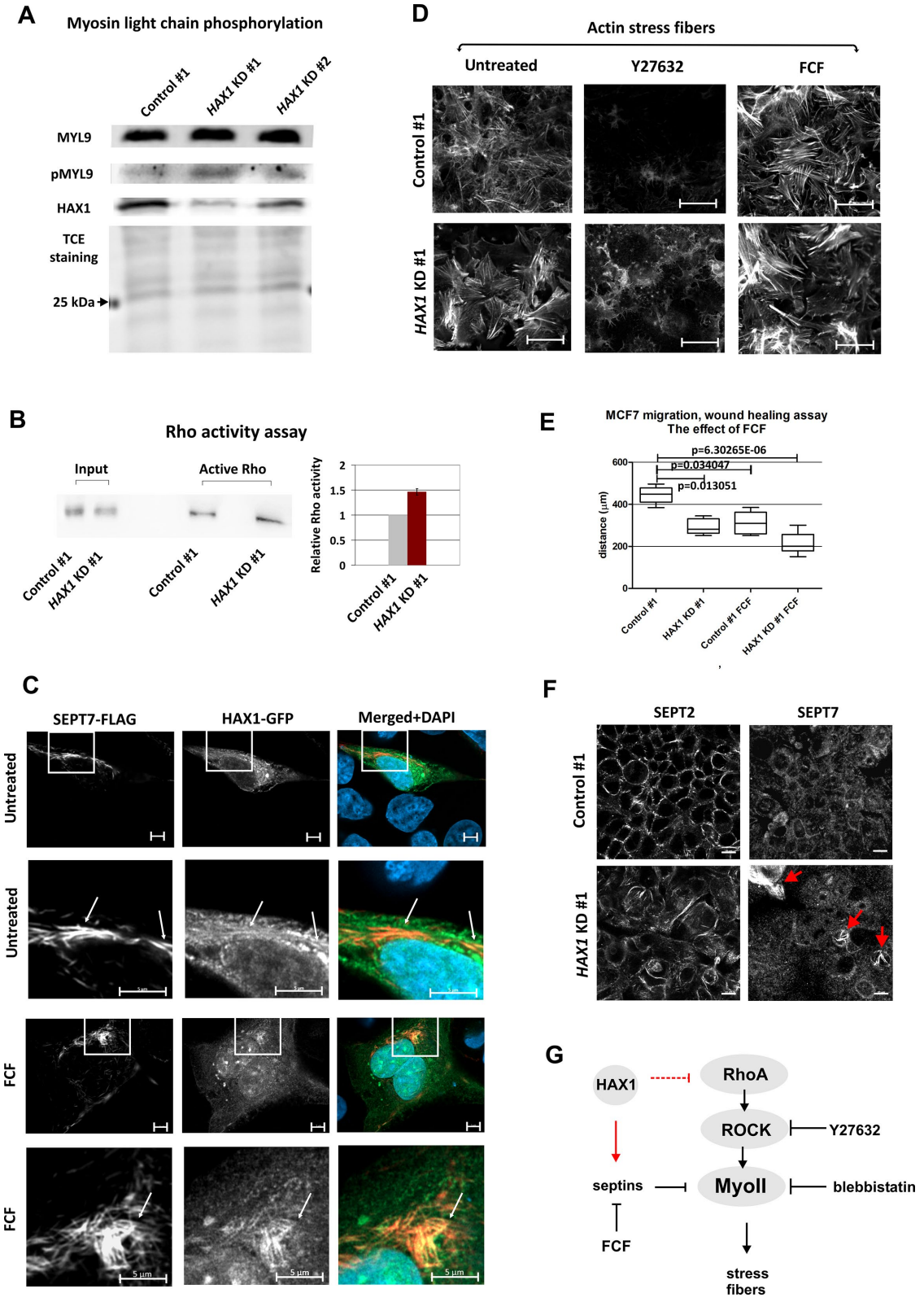

FIGURE 5: HAX1 regulation of actomyosin contractility is mediated by RhoA-ROCK pathway and septins. (A) Myosin light chain 9 phosphorylation is upregulated in HAX1-deficient cells. Western blot with anti-MYL9 (total) and anti-pospho-MYL9 antibodies in the same samples. TCE in-gel protein staining as a loading control. (B) Rho activity assay for *HAX1* KD#1 and control cells (top panel) and relative Rho activity calculated by densitometry from the two assays, error bar: SD (right panel). (C) Partial colocalization of septin 7 and HAX1 in MCF7 cells. Overexpression of SEPT7-Flag and HAX1-GFP. Insets show zoomed versions of boxed areas. Mean Pearson correlation coefficient, respectively, for the untreated and FCF treated cells (5 μM, 18 h): 0.51 ± 0.04, and 0.44 ± 0.03, mean Mander overlap coefficients, respectively: M1 0.73 ± 0.08 and 0.62 ± 0.09, M2 0.21 ± 0.06, and 0.32 ± 0.09, calculated for the whole frame

#	ID	Name	Gene	Score	Peptides	Coverage	Cellular process
1	Q16181	Septin-7	SEPT7	2262.0	14	43.71	Actin dynamics, cell shape, cytokinesis, microtubule regulation (Mostowy and Cossart, 2012), myosin II regulation (Wasik *et al.*, 2017)
2	Q15019	Septin-2	SEPT2	1579.0	10	41.55	Actin dynamics, cell shape, microtubule regulation (Mostowy and Cossart, 2012), scaffold for myosin II (Joo *et al.*, 2007)
3	Q92599	Septin-8	SEPT8	949.0	10	26.5	Septin cytoskeleton
4	Q14244	Ensconsin	MAP7	453.0	8	10.15	Microtubule stabilization (Sun *et al.*, 2011)
5	Q99719	Septin-5	SEPT5	457.0	7	22.22	Platelet biology (Mostowy and Cossart, 2012)
6	Q9NVA2	Septin-11	SEPT11	825.0	6	18.41	Actin dynamics, cell shape, cytokinesis (Mostowy and Cossart, 2012)
7	Q14008	Cytoskeleton-associated protein 5	CKAP5	320.0	5	3.59	Microtubule dynamics, directed migration of breast cancer cells (Chanez *et al.*, 2015), AURKA signaling (Thakur *et al.*, 2014)
8	Q13796	Protein Shroom2	SHROOM2	207.0	5	4.39	Contractility, cell migration (Farber *et al.*, 2011)
9	Q9P0V9	Septin-10	SEPT10	125.0	3	5.07	Septin cytoskeleton
10	O14965	Aurora kinase A	AURKA	141.0	3	8.93	Formation and stabilization of microtubules (Katayama *et al.*, 2008)
11	Q15154	Pericentriolar material 1 protein	PCM1	195.0	3	1.43	Assembly of centrosomal proteins and microtubule organization (Dammermann and Merdes, 2002)

The list represents proteins with the most reliable scores related to the cytoskeleton (11 out of 40 proteins with number of peptides >2). Proteins not related, or loosely related to the ctoskeleton (22) and proteins present in the repository of the most frequent unspecific interaction data (5) (CRAPome [Mellacheruvu *et al.*, 2013]) were eliminated.

TABLE 1: Proteins identified in HAX1-targeted IP with MS/MS detection from MCF7 cells.

HAX1 overexpression

HAX1-overexpressing construct was based on pMK243 (Tet-OsTIR1-PURO from Masato Kanemaki, Addgene plasmid # 72835; Natsume *et al.*, 2016). Original TRE3GS inducible promoter was changed into bidirectional inducible promoter by adding the sequence 5′ ggccgcgatctgacggttcactaaacgagctctgcttatataggcctcccaccgtacacgccacctcgacatac 3′ (this sequence was chosen based on the sequence PTRE3G-B bidirectional inducible promoter from Clontech). The OsTIR1 sequence was replaced with Flag Flag HAX1 sequence (PCR product, *Mlu*I and *Bgl*II restriction sites). For the negative control, only Flag Flag sequence was inserted. A secretable form of luciferase (Gaussia) was cloned from pCMV-Gluc1 plasmid (a gift from Frank Gaunitz, source NanoLight Technology). The presence of secretable luciferase enables monitoring of induction from bidirectional promoter and helps screening the clones during clonal selection. MDA-MB-231 cell line was transfected with *HAX1*-overexpressing construct, and the control construct and the single clones were isolated using puromycin (5 µg/ml) selection.

Migration and invasion assays

A transwell single-cell migration assay was performed on FluoroBlok HTS Multiwell Insert plates with pore sizes of 8 µm (Corning). The 10^5 (MCF7) or 2.5×10^4 (MDA-MB-231) cells were seeded within the apical chamber in 0.5% FBS, migrating toward 10% FBS in the basal chamber. Cells were allowed to migrate for 24 h at 37°C, 5% CO_2 before staining with 4 µg/ml Calcein AM (Molecular Probes) for 1 h at 37°C, 5% CO_2. Fluorescence of migrated cells was measured at 485 nm/535 nm using the Wallac 1420 Multilabel Counter (PerkinElmer).

The invasion assay was performed as above on BioCoat Tumor Invasion System 24-well plates (Corning) coated with BD Matrigel Matrix (BD Biosciences). Results are presented as a percentage of invasion.

Wound healing assay was performed as previously described (Liang *et al.*, 2007). Briefly, a fully confluent cell layer was wounded using a 200-µl pipette tip. A minimum of 20 technical repeats (up to 40) were made for each sample at each time point. The migration distance was photographed and measured at zero time and at indicated time points up to 24 h. Images of the wounded cell monolayers were taken by a light microscope (Olympus IX50) using Quickphoto Camera 2.3 software. Pictures of cells shown in Figure 1C and Supplemental Figure S2A were taken using a JuLI Stage Real-Time Cell History Recorder (NanoEnTek), courtesy of Zygmunt Pojda lab members (Cancer Center, Warsaw, PL). Movies of wound-healing assay were taken using a Zeiss LSM800 confocal microscope.

The Radius 24-well Cell Migration Assay (Cell Biolabs) was performed according to the manufacturer's instructions. Briefly, cells were

(zoomed). Bar: 5 µm. (D) Actin stress fibers in untreated control and HAX1-deficient cells and after Y27632 (10 µM, 1 h) treatment and FCF (5 µM, 18 h) treatment. Bar: 20 µm. (E) The effect of FCF (15 µM, 18 h) on cell migration of control vs. HAX1-deficient cells in wound-healing assay. Statistical significance was assessed by Kruskal–Wallis and Dunn, $n = 8$. (F) Septin fibrils are affected by *HAX1* KD. SEPT2 distribution is more regular in control cells, resembling cortical actin, and more disrupted in HAX1-deficient cells. SEPT7 fibrils are discrete in control cells and occasionally pronounced in HAX1-deficient cells (red arrows). (G) The proposed model depicting the regulation of myosin II by factors affected by HAX1, including RhoA-ROCK pathway and septins. Proposed HAX1 actions marked in red.

seeded at 2.5×10^5 cells/well on collagen I or fibronectin precoated plates and incubated at 37°C, 5% CO_2 for 18 h. After Radius gel removal, cells were allowed to migrate for 7 h. The cell-free area was measured immediately after gel removal and at indicated time points. Cell migration was expressed as the distance covered by the migration front in micrometers, assuming a circular shape of the cell-free area at the beginning and end of the experiment for calculations.

Zymography

Zymography was carried out as in Gogly *et al*. (1998). Briefly, conditioned medium was obtained from 1×10^7 cells starved in serum-free DMEM. Medium was harvested, centrifuged, and concentrated in centriprep tubes: Amicon Ultra-15; Ultracel-10K (Millipore). Samples were loaded into 10% SDS–PAGE containing 0.3 mg/ml collagen I (Sigma). Samples were simultaneously resolved on SDS–PAGE with 0.5% 2,2,2-trichloroethanol (TCE) providing loading control.

Dispase assay

Cells were plated onto six-well plates and on day 4 after reaching confluence, they were washed with phosphate-buffered saline and incubated with dispase II (2.4 U/ml; Roche) for 50 min at 37°C, 5% CO_2, which caused the detachment of the whole monolayers. The plates were sealed with parafilm, placed on a rotator, and subjected to 5, 10, and 40 inversions. Images of fragmented sheets were acquired using a Mini HD4 camera (UVTech Cambridge).

Calcium switch

Mature (6 d), confluent cell layers were cultured in standard DMEM and treated with 4 mM EGTA for 30 min with the medium then replaced with high calcium DMEM (3.8 mM) for 30 min and 1 h. The cells were fixed and observed at all stages.

Immunofluorescence

Immunofluorescence was performed as described previously (Grzybowska *et al*., 2013). Primary antibodies to junction plakoglobin (rabbit, 1:400; Cell Signaling; or mouse, 1:400; Thermo Fisher Scientific), E-cadherin (mouse, 1:100; Pierce), paxillin (rabbit, 1:250, Y113; Abcam), anti-FLAG (1:500, M2; Sigma), septin 2 (rabbit, 1: 100; Thermo Fisher Scientific), and septin 7 (rabbit, 1: 100; Thermo Fisher Scientific) and secondary antibodies goat anti-rabbit Alexa Fluor 594 (1:500; Thermo Fisher Scientific) and donkey anti-mouse Alexa Fluor 647 (1:1000; Abcam) were used. Phalloidin-TRITC conjugate (Sigma, 1:400) was used for labeling actin. Transfections were performed using TurboFect (Thermo Fisher Scientific). Cells were observed using the Zeiss LSM 800 confocal microscope. Images represent single Z-stacks. For HAX1-SEPT7, colocalization Airyscan detector was used.

Focal adhesion measurements

On day 2 after reaching confluence, cells were fixed and immunostained with anti-paxillin antibody. The number and size of focal adhesions were counted using ImageJ for 20 images per cell line (~110 nuclei per image). For quantification, images were split into single-color channels and the background was subtracted by a sliding paraboloid algorithm with radius of 50 pixels. An area of objects larger than 20 square pixels was measured by the Analyze Particles ImageJ built-in function. The number of nuclei was counted by the Nucleus Counter ImageJ built-in function.

CSI

Areas and perimeters of shaped cells were measured using ImageJ on junction plakoglobin-stained images and used to calculate the CSI by the formula: $CSI = 4\pi \times area/(perimeter)^2$. The CSI assumes values between 1 (circular) and 0 (elongated).

Colocalization

Colocalization was assessed using ImageJ JACoP. PCC and the two Mander's overlap coefficients with threshold adjustments were calculated for the entire area (5–12 fields of vision; 1–4 cells/1 field).

Western blot

Western blot was performed as previously described (Grzybowska *et al*., 2013). The following antibodies were used: primary antibodies: junction plakoglobin (rabbit, 1:400; Cell Signaling), E-cadherin (mouse, 1:100; Pierce), MYL9 (rabbit, 1:1000; Thermo Fisher Scientific) and pMYL9 (rabbit, 1:250; Thermo Fisher Scientific), and HAX1 (mouse, 1:250; BD Biosciences); HRP–conjugated secondary antibodies: goat anti-mouse (1:10,000; Pierce) or goat anti-rabbit (1:10,000; Abcam). WesternBright Quantum (Advansta) was used in the assays. To confirm equal protein loading, blots were probed with antibodies to β-actin (mouse, HRP–conjugated, 1:1000; Cell Signaling) or to α-tubulin (rabbit, HRP-conjugated, 1:1000; Cell Signaling).

Rho activity assay

A total of 9×10^6 of MCF-7 *HAX1* KD and control cells were seeded onto 100-mm dishes, starved overnight in DMEM with 0.25% FBS, and incubated in standard growth medium for 8 min. Rho activity was assessed using the Active Rho Pull-Down and Detection Kit (Thermo Fisher Scientific) according to the manufacturer's protocol.

Mass spectrometry

Sample preparation for proteome analysis. MCF7 cells (7.5×10^6) were used per one IP experiment. The experiment was performed in triplicate. Cells were permeabilized with lysis buffer (150 mM NaCl, 50 mM Tris–HCl, pH 7.5, 5 mM EDTA, pH 8.0, 0.5% Nonidet P-40, 1% Triton X-100; protease and phosphatase inhibitors Halt Protease and Phosphatase Inhibitor Cocktail; Thermo Fisher Scientific) and harvested using a cell scraper. Cell lysate was pulled 10× through a 29-G needle, centrifuged at $12,000 \times g$ for 15 min at 4°C, and subjected to immunoaffinity chromatography via magnetic bead extraction using 10 µg of anti-HAX1 rabbit polyclonal antibody (Thermo Fisher Scientific) and anti–immunoglobulin G rabbit polyclonal antibody (Sigma, negative control) coupled to dynabeads protein A (1.5 mg; Thermo Fisher Scientific). IP was carried out overnight at 4°C with gentle rotation. Beads with antigen–antibody complexes were collected using magnetic separation method and washed 4× in a wash buffer (50 mM Tris–HCl, pH 7.4, 150 mM NaCl, 0.5% Nonidet P-40), the last wash without detergent. Proteins bound to beads were reduced with 5 mM Tris(2-carboxyethyl) phosphine (60°C, 1 h), methylthiolated with 10 mM *S*-methyl methanethiosulfonate (room temperature, 10 min) to block cysteine residues, and digested overnight at 37°C with trypsin (Promega) added at 1:20 vol/vol ratio.

MS measurement and data processing. LC-MS/MS (liquid chromatography–mass spectrometry) measurements were performed on a QExactive mass spectrometer (Thermo Fisher Scientific) coupled with a nanoACQUITY LC system (Waters). The sample was desalted and concentrated on a nanoACQUITY UPLC Trapping Column (Waters), and further peptide separation was carried on a nanoACQUITY UPLC BEH C18 Column (75 µm inner diameter and 250 mm long; Waters) with an ACN gradient (5–30% over 120 min) in the presence of 0.1% formic acid at a flow rate of 250 nl/min. The column outlet was

directly connected to the electrospray ion source of the mass spectrometer. Preprocessed MS/MS data files were submitted to the Mascot search engine (Matrix Science) and searched against human protein entries from the SwissProt (2017.04) database using a target/decoy approach. The search parameters were as follows: enzyme, semitrypsin; number of missed cleavages, 1; ion mass error tolerances, ±5 ppm (parent) and ± 0.01 Da (fragment); modifications, Methylthio C (fixed) and Oxidation M (variable). The statistical significance of the identifications was assessed as previously described (Mikula *et al*., 2010). Only peptide sequences with q values ≤ 0.01 were regarded as confidently identified, and proteins represented by less than three peptides were excluded from further analysis.

The mass spectrometry proteomics data have been deposited to the ProteomeXchange Consortium via the PRIDE (Vizcaino *et al*., 2016) partner repository with the data set identifier PXD007888 and 10.6019/PXD007888.

Protein interactions were analyzed using STRING.

Statistical analysis

Statistical inference for migration assays was performed by nonparametric Mann–Whitney test for two groups, nonparametric Kruskal–Wallis and post-hoc Dunn test, one-way analysis of variance (ANOVA) and post-hoc test Tukey (multiple groups), or one-way ANOVA and planned contrast analysis (group comparison). Statistical significance in fragmentation assay was assessed using a two-tailed Student's t test. Statistical inference for adhesion studies was assessed by one-way ANOVA and post-hoc Tukey test. Distribution was assessed by Kolmogorow–Smirnov two-sample test. Cumulative distribution frequency plots were created using GraphPad Prism version 6.07 for Windows (GraphPad Software, La Jolla CA, www.graphpad.com).

ACKNOWLEDGMENTS

This work was supported by the Polish National Science Center under grants 2011/01/B/NZ1/03674, 2014/14/M/NZ1/00437, and 2015/17/N/NZ5/01392.

REFERENCES

Aceto N, Bardia A, Miyamoto DT, Donaldson MC, Wittner BS, Spencer JA, Yu M, Pely A, Engstrom A, Zhu H, *et al*. (2014). Circulating tumor cell clusters are oligoclonal precursors of breast cancer metastasis. Cell 158, 1110–1122.

Al-Maghrebi M, Brule H, Padkina M, Allen C, Holmes WM, Zehner ZE (2002). The 3′ untranslated region of human vimentin mRNA interacts with protein complexes containing eEF-1gamma and HAX-1. Nucleic Acids Res 30, 5017–5028.

Bachir AI, Horwitz AR, Nelson WJ, Bianchini JM (2017). Actin-based adhesion modules mediate cell interactions with the extracellular matrix and neighboring cells. Cold Spring Harb Perspect Biol 9, 10.1101/cshperspect.a023234.

Burridge K, Guilluy C (2016). Focal adhesions, stress fibers and mechanical tension. Exp Cell Res 343, 14–20.

Campbell K, Casanova J (2016). A common framework for EMT and collective cell migration. Development 143, 4291–4300.

Cavnar PJ, Berthier E, Beebe DJ, Huttenlocher A (2011). Hax1 regulates neutrophil adhesion and motility through RhoA. J Cell Biol 193, 465–473.

Chanez B, Goncalves A, Badache A, Verdier-Pinard P (2015). Eribulin targets a ch-TOG-dependent directed migration of cancer cells. Oncotarget 6, 41667–41678.

Chao JR, Parganas E, Boyd K, Hong CY, Opferman JT, Ihle JN (2008). Hax1-mediated processing of HtrA2 by Parl allows survival of lymphocytes and neurons. Nature 452, 98–102.

Cheung KJ, Padmanaban V, Silvestri V, Schipper K, Cohen JD, Fairchild AN, Gorin MA, Verdone JE, Pienta KJ, Bader JS, Ewald AJ (2016). Polyclonal breast cancer metastases arise from collective dissemination of keratin 14-expressing tumor cell clusters. Proc Natl Acad Sci USA 113, E854–E863.

Cilenti L, Soundarapandian MM, Kyriazis GA, Stratico V, Singh S, Gupta S, Bonventre JV, Alnemri ES, Zervos AS (2004). Regulation of HAX-1 anti-apoptotic protein by Omi/HtrA2 protease during cell death. J Biol Chem 279, 50295–50301.

Clark AG, Vignjevic DM (2015). Modes of cancer cell invasion and the role of the microenvironment. Curr Opin Cell Biol 36, 13–22.

Collins C, Nelson WJ (2015). Running with neighbors: coordinating cell migration and cell-cell adhesion. Curr Opin Cell Biol 36, 62–70.

Dammermann A, Merdes A (2002). Assembly of centrosomal proteins and microtubule organization depends on PCM-1. J Cell Biol 159, 255–266.

Farber MJ, Rizaldy R, Hildebrand JD (2011). Shroom2 regulates contractility to control endothelial morphogenesis. Mol Biol Cell 22, 795–805.

Gallagher AR, Cedzich A, Gretz N, Somlo S, Witzgall R (2000). The polycystic kidney disease protein PKD2 interacts with Hax-1, a protein associated with the actin cytoskeleton. Proc Natl Acad Sci USA 97, 4017–4022.

Gogly B, Groult N, Hornebeck W, Godeau G, Pellat B (1998). Collagen zymography as a sensitive and specific technique for the determination of subpicogram levels of interstitial collagenase. Anal Biochem 255, 211–216.

Gomathinayagam R, Muralidharan J, Ha JH, Varadarajalu L, Dhanasekaran DN (2014). Hax-1 is required for Rac1-Cortactin interaction and ovarian carcinoma cell migration. Genes Cancer 5, 84–99.

Grzybowska EA, Zayat V, Konopinski R, Trebinska A, Szwarc M, Sarnowska E, Macech E, Korczynski J, Knapp A, Siedlecki JA (2013). HAX-1 is a nucleocytoplasmic shuttling protein with a possible role in mRNA processing. FEBS J 280, 256–272.

Han Y, Chen YS, Liu Z, Bodyak N, Rigor D, Bisping E, Pu WT, Kang PM (2006). Overexpression of HAX-1 protects cardiac myocytes from apoptosis through caspase-9 inhibition. Circ Res 99, 415–423.

Hidalgo-Carcedo C, Hooper S, Chaudhry SI, Williamson P, Harrington K, Leitinger B, Sahai E (2011). Collective cell migration requires suppression of actomyosin at cell-cell contacts mediated by DDR1 and the cell polarity regulators Par3 and Par6. Nat Cell Biol 13, 49–58.

Hu G, Zhao X, Wang J, Lv L, Wang C, Feng L, Shen L, Ren W (2018). miR-125b regulates the drug-resistance of breast cancer cells to doxorubicin by targeting HAX-1. Oncol Lett 15, 1621–1629.

Joo E, Surka MC, Trimble WS (2007). Mammalian SEPT2 is required for scaffolding nonmuscle myosin II and its kinases. Dev Cell 13, 677–690.

Katayama H, Sasai K, Kloc M, Brinkley BR, Sen S (2008). Aurora kinase-A regulates kinetochore/chromatin associated microtubule assembly in human cells. Cell Cycle 7, 2691–2704.

Klein C, Grudzien M, Appaswamy G, Germeshausen M, Sandrock I, Schaffer AA, Rathinam C, Boztug K, Schwinzer B, Rezaei N, *et al*. (2007). HAX1 deficiency causes autosomal recessive severe congenital neutropenia (Kostmann disease). Nat Genet 39, 86–92.

Kwiecinska A, Ottosson-Wadlund A, Ceder R, Grafstrom RC, Bjorck E, Nordenskjold M, Porwit A, Fadeel B (2011). HAX-1 expression in human B lymphoma. Leukemia 25, 868–872.

Li DS, Zimmermann J, Levine H (2016). Modeling closure of circular wounds through coordinated collective motion. Phys Biol 13, 016006.

Li M, Tang Y, Zang W, Xuan X, Wang N, Ma Y, Wang Y, Dong Z, Zhao G (2013). Analysis of HAX-1 gene expression in esophageal squamous cell carcinoma. Diagn Pathol 8, 47.

Li X, Li T, You B, Shan Y, Shi S, Cao X, Qian L (2015). Expression and function of HAX-1 in human cutaneous squamous cell carcinoma. J Cancer 6, 351–359.

Liang CC, Park AY, Guan JL (2007). In vitro scratch assay: a convenient and inexpensive method for analysis of cell migration in vitro. Nat Protoc 2, 329–333.

Liu H, Yue J, Huang H, Gou X, Chen SY, Zhao Y, Wu X (2015). Regulation of focal adhesion dynamics and cell motility by the EB2 and Hax1 protein complex. J Biol Chem 290, 30771–30782.

Mekkawy AH, Morris DL, Pourgholami MH (2011). HAX1 augments cell proliferation, migration, adhesion, and invasion induced by urokinase-type plasminogen activator receptor. J Oncol 2012, 950749.

Mellacheruvu D, Wright Z, Couzens AL, Lambert JP, St-Denis NA, Li T, Miteva YV, Hauri S, Sardiu ME, Low TY, *et al*. (2013). The CRAPome: a contaminant repository for affinity purification-mass spectrometry data. Nat Methods 10, 730–736.

Mikula M, Gaj P, Dzwonek K, Rubel T, Karczmarski J, Paziewska A, Dzwonek A, Bragoszewski P, Dadlez M, Ostrowski J (2010). Comprehensive analysis of the palindromic motif TCTCGCGAGA: a regulatory element of the HNRNPK promoter. DNA Res 17, 245–260.

Mirmohammadsadegh A, Tartler U, Michel G, Baer A, Walz M, Wolf R, Ruzicka T, Hengge UR (2003). HAX-1, identified by differential display

reverse transcription polymerase chain reaction, is overexpressed in lesional psoriasis. J Invest Dermatol 120, 1045–1051.
Mostowy S, Cossart P (2012). Septins: the fourth component of the cytoskeleton. Nat Rev Mol Cell Biol 13, 183–194.
Natsume T, Kiyomitsu T, Saga Y, Kanemaki MT (2016). Rapid protein depletion in human cells by auxin-inducible degron tagging with short homology donors. Cell Rep 15, 210–218.
Pedersen K, Canals F, Prat A, Tabernero J, Arribas J (2014). PELO negatively regulates HER receptor signalling and metastasis. Oncogene 33, 1190–1197.
Radhika V, Onesime D, Ha JH, Dhanasekaran N (2004). Galpha13 stimulates cell migration through cortactin-interacting protein Hax-1. J Biol Chem 279, 49406–49413.
Ramsay AG, Keppler MD, Jazayeri M, Thomas GJ, Parsons M, Violette S, Weinreb P, Hart IR, Marshall JF (2007). HS1-associated protein X-1 regulates carcinoma cell migration and invasion via clathrin-mediated endocytosis of integrin alphavbeta6. Cancer Res 67, 5275–5284.
Sheng C, Ni Q (2015). Expression of HAX1 and Ki-67 in breast cancer and its correlations with patient's clinicopathological characteristics and prognosis. Int J Clin Exp Med 8, 20904–20910.
Smith C, Dolat L, Angelis D, Forgacs E, Spiliotis ET, Galkin VE (2015). Septin 9 exhibits polymorphic binding to F-actin and inhibits myosin and cofilin activity. J Mol Biol 427, 3273–3284.
Spiliotis ET, Gladfelter AS (2012). Spatial guidance of cell asymmetry: septin GTPases show the way. Traffic 13, 195–203.
Sun SJ, Feng L, Zhao GQ, Dong ZM (2012). HAX-1 promotes the chemoresistance, invasion, and tumorigenicity of esophageal squamous carcinoma cells. Dig Dis Sci 57, 1838–1846.
Sun X, Shi X, Liu M, Li D, Zhang L, Liu X, Zhou J (2011). Mdp3 is a novel microtubule-binding protein that regulates microtubule assembly and stability. Cell Cycle 10, 3929–3937.
Thakur HC, Singh M, Nagel-Steger L, Kremer J, Prumbaum D, Fansa EK, Ezzahoini H, Nouri K, Gremer L, Abts A, *et al.* (2014). The centrosomal adaptor TACC3 and the microtubule polymerase chTOG interact via defined C-terminal subdomains in an Aurora-A kinase-independent manner. J Biol Chem 289, 74–88.
Thompson EW, Paik S, Brunner N, Sommers CL, Zugmaier G, Clarke R, Shima TB, Torri J, Donahue S, Lippman ME, *et al.* (1992). Association of increased basement membrane invasiveness with absence of estrogen receptor and expression of vimentin in human breast cancer cell lines. J Cell Physiol 150, 534–544.
Trebinska A, Hogstrand K, Grandien A, Grzybowska EA, Fadeel B (2014). Exploring the anti-apoptotic role of HAX-1 versus BCL-XL in cytokine-dependent bone marrow-derived cells from mice. FEBS Lett 588, 2921–2927.
Trebinska A, Rembiszewska A, Ciosek K, Ptaszynski K, Rowinski S, Kupryjanczyk J, Siedlecki JA, Grzybowska EA (2010). HAX-1 overexpression, splicing and cellular localization in tumors. BMC Cancer 10, 76.
Vizcaino JA, Csordas A, del-Toro N, Dianes JA, Griss J, Lavidas I, Mayer G, Perez-Riverol Y, Reisinger F, Ternent T, *et al.* (2016). 2016 update of the PRIDE database and its related tools. Nucleic Acids Res 44, D447–D456.
Wang Y, Huo X, Cao Z, Xu H, Zhu J, Qian L, Fu H, Xu B (2015). HAX-1 is overexpressed in hepatocellular carcinoma and promotes cell proliferation. Int J Clin Exp Pathol 8, 8099–8106.
Wasik AA, Dumont V, Tienari J, Nyman TA, Fogarty CL, Forsblom C, Lehto M, Lehtonen E, Groop PH, Lehtonen S (2017). Septin 7 reduces non-muscle myosin IIA activity in the SNAP23 complex and hinders GLUT4 storage vesicle docking and fusion. Exp Cell Res 350, 336–348.
Wei XJ, Li SY, Yu B, Chen G, Du JF, Cai HY (2014). Expression of HAX-1 in human colorectal cancer and its clinical significance. Tumour Biol 35, 1411–1415.
Yan J, Ma C, Cheng J, Li Z, Liu C (2015). HAX-1 inhibits apoptosis in prostate cancer through the suppression of caspase-9 activation. Oncol Rep 34, 2776–2781.
Yang J, Wu Y, Wang X, Xu L, Zhao X, Yang Y (2017). Chemoresistance is associated with overexpression of HAX-1, inhibition of which resensitizes drug-resistant breast cancer cells to chemotherapy. Tumour Biol 39, 1010428317692228.
Zayat V, Balcerak A, Korczynski J, Trebinska A, Wysocki J, Sarnowska E, Chmielarczyk M, Macech E, Konopinski R, Dziembowska M, Grzybowska EA (2015). HAX-1: a novel p-body protein. DNA Cell Biol 34, 43–54.
Zhang Y, Zhang XF, Fleming MR, Amiri A, El-Hassar L, Surguchev AA, Hyland C, Jenkins DP, Desai R, Brown MR, *et al.* (2016). Kv3.3 channels bind Hax-1 and Arp2/3 to assemble a stable local actin network that regulates channel gating. Cell 165, 434–448.